Nuclear Instruments and Methods in Physics Research B 268 (2010) 28–35

Contents lists available at ScienceDirect

Nuclear Instruments and Methods in Physics Research B

journal homepage: www.elsevier.com/locate/nimb

Gas phase chemical studies of superheavy elements using the Dubna gas-filled recoil separator – Stopping range determination

D. Wittwer [a,b,*], F.Sh. Abdullin [c], N.V. Aksenov [c], Yu.V. Albin [c], G.A. Bozhikov [c], S.N. Dmitriev [c], R. Dressler [b], R. Eichler [a,b], H.W. Gäggeler [a,b], R.A. Henderson [d], S. Hübener [e], J.M. Kenneally [d], V.Ya. Lebedev [c], Yu.V. Lobanov [c], K.J. Moody [d], Yu.Ts. Oganessian [c], O.V. Petrushkin [c], A.N. Polyakov [c], D. Piguet [b], P. Rasmussen [b], R.N. Sagaidak [c], A. Serov [a,b], I.V. Shirokovsky [c], D.A. Shaughnessy [d], S.V. Shishkin [c], A.M. Sukhov [c], M.A. Stoyer [d], N.J. Stoyer [d], E.E. Tereshatov [c], Yu.S. Tsyganov [c], V.K. Utyonkov [c], G.K. Vostokin [c], M. Wegrzecki [f], P.A. Wilk [d]

[a] Departement für Chemie und Biochemie, Universität Bern, CH-3012 Bern, Switzerland
[b] Labor für Radio-und Umweltchemie, Paul Scherrer Institut, CH-5232 Villigen, Switzerland
[c] Flerov Laboratory of Nuclear Reactions, Joint Institute for Nuclear Research, 141980 Dubna, Russia
[d] Lawrence Livermore National Laboratory, Livermore, CA 94551, USA
[e] Forschungszentrum Dresden Rossendorf, D-01314 Dresden, Germany
[f] Institute of Electron Technology, PL-02-668 Warsaw, Poland

ARTICLE INFO

Article history:
Received 14 August 2009
Received in revised form 30 September 2009
Available online 12 October 2009

PACS:
61.85.+p
27.90.+b
25.70.−z
29.30.−h

Keywords:
Heavy ion
Stopping force
Mylar
Argon
Superheavy elements
Physical preseparator

ABSTRACT

Currently, gas phase chemistry experiments with heaviest elements are usually performed with the gas-jet technique with the disadvantage that all reaction products are collected in a gas-filled thermalisation chamber adjacent to the target. The incorporation of a physical preseparation device between target and collection chamber opens up the perspective to perform new chemical studies. But this approach requires detailed knowledge of the stopping force (STF) of the heaviest elements in various materials. Measurements of the energy loss of mercury (Hg), radon (Rn), and nobelium (No) in Mylar and argon (Ar) were performed at low kinetic energies of around (40–270) keV per nucleon. The experimentally obtained values were compared with STF calculations of the commonly used program for calculating stopping and ranges of ions in matter (SRIM). Using the obtained data points an extrapolation of the STF up to element 114, eka-lead, in the same stopping media was carried out. These estimations were applied to design and to perform a first chemical experiment with a superheavy element behind a physical preseparator using the nuclear fusion reaction ^{244}Pu(^{48}Ca; 3n)^{289}114. One decay chain assigned to an atom of ^{285}112, the α-decay product of ^{289}114, was observed.

1. Introduction

The experimental determination of physical and chemical properties of the heaviest known elements represents an interesting and challenging topic in the current nuclear chemistry and nuclear physics research. The irradiation of actinide targets with intense beams of ^{48}Ca is so far the most successful way to produce the heaviest elements in nuclear fusion reactions, for review see [1].

Chemistry experiments with superheavy elements formed in complete fusion reactions are usually performed with the gas-jet technique where all reaction products are collected in a gas-filled thermalisation chamber adjacent to the target and transported as gaseous species or attached to aerosols. This technique has the disadvantage that very high chemical separation factors are required to isolate and identify single atoms of very heavy elements from the bulk of other reaction products. For an overview on chemistry experiments employing heavy ion induced nuclear fusion reactions we refer to [2].

The incorporation of a physical preseparation device between target and collection chamber opens up the perspective to perform much cleaner and partly novel chemical studies [3,4]. Magnetic and electrostatic separators [5–10] can be applied to physically separate the recoiling evaporation residues (EVR's) via kinematic

* Corresponding author. Address: Paul Scherrer Institut, OFLB 105, CH-5232 Bern, Switzerland. Tel.: +41 56 310 24 68; fax: +41 56 310 44 35.
E-mail address: david.wittwer@psi.ch (D. Wittwer).

0168-583X/$ - see front matter © 2009 Elsevier B.V. All rights reserved.
doi:10.1016/j.nimb.2009.09.062

selection from vast amounts of by-products of the nuclear reaction prior to entering a chemistry setup.

The coupling of a gas-filled recoil separator [11] to a chemical separation scheme has been performed for the first time at the Berkeley Gas-filled Separator (BGS) [7] at the Lawrence Berkeley National Laboratory (LBNL), Berkeley, USA. Recently, such couplings are under development at the Transactinide Separator and Chemistry Apparatus (TASCA) [10] at the Gesellschaft für Schwerionenforschung (GSI), Darmstadt, Germany, at the gas-filled recoil ion separator (GARIS) [9] at RIKEN, Wako, Japan, and at the gas-filled recoil separator (DGFRS) [8] at the Flerov Laboratory of Nuclear Reactions (FLNR) in Dubna, Russia. All these gas-filled separators allow for a momentum separation of unwanted reaction products in a gas-filled magnet array (typically pressure 50–150 Pa H_2 or He). A gas catcher that stops the EVRs is installed then in the ion optical focal plane of the separator. Products stopped in the catcher can be subjected to further chemical separation procedures permitting a nearly background-free detection.

One drawback of this technique is the decrease of sensitivity induced by the limited transmission of the physical separator and the lower production rates due to limited target thicknesses applicable at physical separators. Due to the pressure difference between the gas-filled separator and the gas catcher, a physical divider in form of a window foil must be introduced. This foil has to withstand the applied pressure differences but has to be also thin enough to efficiently let pass the low energy EVR's. Moreover, the foil and the gas conditions in the catcher need to be adjusted to thermalize the EVR's in a gas volume as small as possible to keep the further transport as fast as possible. Hence, such a combination of a physical preseparator and a chemical separation demands a detailed knowledge of the STF from involved ions.

Recently, the "in situ volatilization and on-line detection" (IVO) technique [12–14] was used to investigate the chemical behavior of element 112, eka-mercury. Here we describe the first experiment to investigate element 114, eka-lead, via coupling of this IVO-system to the DGFRS as a physical preseparator. We will first discuss STF-measurements of Hg, Rn, and No in Mylar and gaseous Ar performed in preparation of the main experiment. Secondly, the extrapolative method to estimate the STF of element 114 in Mylar and Ar will be explained. Finally, the results obtained in an experiment using the nuclear fusion reaction $^{48}Ca + ^{244}Pu$ to synthesize element 114 will be presented.

2. Materials and methods

2.1. Stopping force experiment

A (265 ± 3) MeV $^{48}Ca^{18+}$ beam delivered from the U-400 cyclotron at the Joint Institute for Nuclear Research (JINR) in Dubna, Russia, in combination with the rotating target wheel setup of the DGFRS (see e.g. [15]) was used to perform all irradiations. Three different target materials were irradiated to determine the STF's of Hg, Rn, and No. The targets were made of neodymium oxide ($^{nat}Nd_2O_3$, 0.35 mg/cm^2), dysprosium oxide ($^{nat}Dy_2O_3$, 0.38 mg/cm^2), and lead (^{208}Pb, 0.42 mg/cm^2), respectively. The lanthanide targets were prepared via electroplating on arc-shaped Ti segments of 0.73 mg/cm^2 thickness, whereas the lead target was deposited by vapor deposition on arc-shaped Cu segments (1.09 mg/cm^2). The Hg and Rn experiments were performed using a mixed target wheel containing two Nd, two Dy, and two empty Ti segments. The beam was chopped to the wanted targets to separately produce either Hg or Rn isotopes. The beam energy in the center of the targets was (244 ± 3) MeV in the Hg and Rn experiments. In the case of the No experiments the whole target wheel was equipped with ^{208}Pb segments and an additional degrader foil of 1.40 mg/cm^2 Al was installed prior to the target to reduce the beam energy to (217 ± 3) MeV in the center of the target. The evaporation residues mainly produced are according to HIVAPSI [16] ^{185}Hg, ^{206}Rn, and ^{254}No, formed in the fusion reactions $^{142}Nd(^{48}Ca; 5n)^{185}Hg$, $^{164}Dy(^{48}Ca; 6n)^{206}Rn$, and $^{208}Pb(^{48}Ca; 2n)^{254}No$, respectively. The HIVAPSI program is a statistical code based on the Hauser Feshbach formalism to estimate the production-cross-section of compound nuclei formation with followed particle evaporation. Beam intensities between 1.5×10^{11} particles per second and 1.4×10^{12} particles per second (i.e. 24×10^{-9} pA–220×10^{-9} pA) were applied. The evaporation residues were guided through the DGFRS towards an aluminized Mylar foil of 2.0 μm, 3.0 μm, or 5.0 μm (± 5%, 2σ c.i., i.e. 95.45% confidence interval) thickness separating the reaction product collection chamber (RPC-chamber) from the gas-filled magnet array of DGFRS. The RPC-chamber had

Table 1
Experimental conditions applied during measurements.

		Mylar thickness in μm		
		2.00 ± 0.10	3.00 ± 0.15	5.00 ± 0.25
Ar pressure [kPa]	0	Hg, Rn, No	No	Hg, Rn
	20 ± 2	Hg, Rn, No	–	–
	40 ± 2	Hg, Rn	–	–

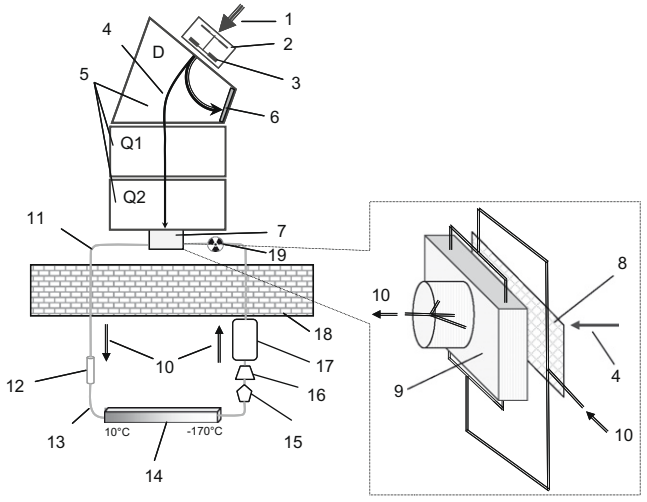

Fig. 1. Schematic of the experimental setup using physical preseparation with the DGFRS. The ^{48}Ca beam (1) passes through a rotating target assembly consisting of a Ti vacuum window (2) and a target backing (3) before entering the target material ($^{244}PuO_2$) which was electroplated on Ti backing foils. The beam (1) and nuclear reaction products (4) entering the cavity of the DGFRS magnet array (5: D, Q1, Q2, 133 Pa H_2). They are spatially separated in the gas-filled dipole magnet (D). The beam (low rigidity ions) is redirected to the Ta beam dump (6). Only nuclear reaction products having the required magnetic rigidity are focused by the two quadruple lenses (Q1, Q2) onto the focal plane (7) of the separator. Here, the products pass through a 3.0 μm thick Mylar window (8) mounted on a honey comb steel grid (80% transitivity) and are stopped in the Ar filled RPC-chamber (9). The carrier gas Ar (10) transports the thermalized products through a 4 m long perfluoroalkoxy-Teflon (PFA) capillary (1.56 mm inner diameter) (11) to a quartz column containing tantalum metal and a quartz wool plug, both heated up to 850 °C (12), serving as a getter/trap for water, oxygen, and other reactive species. Volatile and inert nuclear reaction products pass this getter and are transferred further through a 40 cm PFA capillary (13) (2 mm inner diameter) to the thermochromatographic detection system COLD (14). The gas flow within the closed loop system was established by metal bellow pumps (16). The gas loop consists of a drying unit (15) for additionally purification of the gas and a buffer volume (17) to prevent pressure waves and variations of the flow rate. Between the separator and COLD a concrete wall (18) of 2 m thickness shielded the sensitive spectroscopy electronics from fast particles produced by beam-induced nuclear processes. An ^{227}Ac source (19) flushed by the carrier gas was mounted in front of the recoil chamber.

a height of 30 mm and a width of 100 mm, both measures adjusted to the EVR image size in the focal plane image of the DGFRS [17]. An RPC-chamber with a depth of 20 mm was selected for the experiments of the STF determination. This RPC-chamber could be evacuated and subsequently filled with Ar gas up to a chosen pressure. At the back wall of this chamber a silicon detector (PIN-diode, 20 mm × 20 mm) was mounted and operated at 40 V reverse bias voltage to detect the implantation signals from separated EVR's as well as their emitted α particles. Due to the thickness of this detector the effective depth of the RPC-chamber was reduced to 18 mm. The detector was calibrated using the α-lines of the product isotopes ^{185}Hg (5.65 MeV), ^{206}Rn (6.26 MeV), and ^{254}No (8.10 MeV), respectively. The separator settings were optimal for the ^{208}Pb(^{48}Ca; 2n)^{254}No reaction corresponding to magnetic rigidity of 2.12 Tm and were chosen in a way to minimize scattered beam particles for the two other reactions (1.73 Tm). Therefore, only a part of the produced Hg and Rn EVR's reached the RPC-chamber. These settings avoided an overload of the PIN detector. The measurements were started without Mylar foil, i.e. at DGFRS pressure conditions (133 Pa H_2) within the RPC-chamber. Subsequently both, the Mylar (density: 1.397 g/cm^3) foil thickness and the Ar (density: 1.784 mg/cm^3) pressure in the RPC-chamber were varied during consecutive experiments. The parameters of these experiments are listed in Table 1. The Mylar foil was mounted on a honeycomb grid with 6 mm gap size and 0.75 mm web thickness to support the foil resulting in a transmission of 80%. All measurements used to determine the STF's in Ar were performed using a 2.0 μm Mylar window foil (second column in Table 1). The 2σ uncertainties of the Mylar foil thicknesses were determined by weighing 50 equally sized circular foils of nominally 2.0 and 5.0 μm thickness. This procedure results in an expected 2σ c.i. of 5% for all used foils. The uncertainty of the pressure measurement is estimated to be about 5% as well. For all relevant calculations an absolute uncertainty of 0.25 μm for all the Mylar thicknesses and 2 kPa for all Ar pressures were used. This is a conservative uncertainty estimation which regards to the unknown stretching and bending behavior of the foil under the pressure differences.

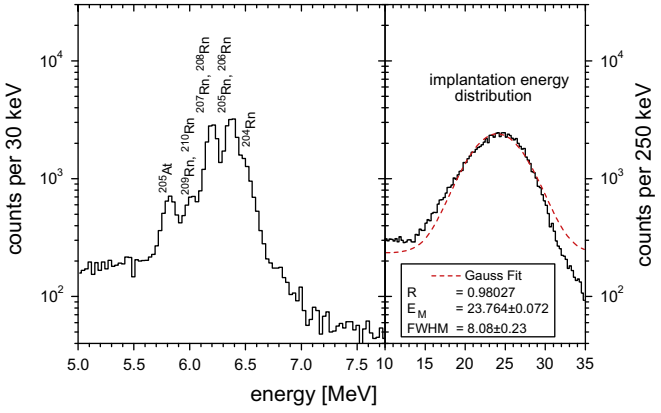

Fig. 2. Recorded spectrum during a run with the Dy target at 133 Pa H_2 in the separator and in the RPC-chamber. No Mylar foil was installed. On the left side the α-spectrum of the produced isotopes is shown. The implantation energy distribution of the EVR's is shown on the right side of the spectrum in the high energy region together with a Gaussian fit (dashed line) to determine the mean energy (E_M) and the FWHM of the EVR's. R is the regression coefficient.

2.2. Experiment with element 114

The experiments investigating the chemical properties of element 114 were carried out using targets of $^{244}PuO_2$ (0.44 mg/cm^2 of ^{244}Pu) deposited on arc-shaped Ti backing foils (725 μg/cm^2) which were irradiated with an intense ^{48}Ca beam of (265 ± 3) MeV primary energy from the U-400 cyclotron. The energy of the beam in the middle of the target was calculated using SRIM-2008 [18] to be (243 ± 3) MeV. The beam dose accumulated on the target during 35 days was 9.7 × 10^{18} particles. The magnet settings of

Table 3
STF data and ranges for isotopes ^{185}Hg, ^{206}Rn, and ^{254}No, respectively. The upper part shows the STF values and ranges in Mylar. The lower part shows the STF values and ranges in gaseous Ar.

In Mylar		Hg	Rn	No
E_I	[MeV]	48.7 ± 7.8	46.7 ± 7.6	29.0 ± 4.8
STF	[MeV/(mg/cm^2)]	33.8 ± 6.0	34.7 ± 4.8	24.83 ± 0.35
STF-SRIM-2008	[MeV/(mg/cm^2)]	42.3 ± 4.6	40.1 ± 5.6	26.89 ± 0.58
Range	[μm]	10.3 ± 2.5	9.6 ± 2.1	8.4 ± 1.4
Range-SRIM-2008	[μm]	8.2 ± 1.6	8.3 ± 1.8	7.7 ± 1.3
In Ar		**Hg**	**Rn**	**No**
E_I	[MeV]	37.3 ± 7.2	35.5 ± 7.0	22.2 ± 4.4
STF	[MeV/(mg/cm^2)]	12.5 ± 1.1	11.4 ± 1.6	10.1 ± 1.6[a]
STF-SRIM-2008	[MeV/(mg/cm^2)]	22.2 ± 1.5	20.1 ± 1.8	17.7 ± 1.8[a]
Range at 101 kPa	[cm]	1.7 ± 1.0	1.7 ± 1.0	1.2 ± 1.0[a]
Range-SRIM-2008	[cm]	1.20 ± 0.25	1.26 ± 0.27	0.90 ± 0.27[a]

[a] STF and range uncertainties for No in Ar are estimated maximal values.

Table 2
The measured and calculated initial data used for the STF determination. *PF* is the prefactor from Eq. (3). E_M is the measured implantation signal (mean energy). FWHM is the full width at half maximum indicating the width of the energy distribution of the recorded EVR's. E_I is the PHD corrected incident energy used to determine the STF's of the EVR's. d_{Mylar} and p_{Ar} are the Mylar thickness and the argon pressure, respectively.

EVR	d_{Mylar} [μm]	p_{Ar} [kPa]	*PF* [MeV]$^{1/2}$	E_M [MeV]	FWHM [MeV]	E_I [MeV]
^{185}Hg	0	0	3.13 ± 0.86	26.805 ± 0.078[a]	8.56 ± 0.26	48.7 ± 7.8[b]
^{185}Hg	2	0	3.13 ± 0.86	18.157 ± 0.068	5.82 ± 0.26	37.3 ± 7.3
^{185}Hg	2	20	3.13 ± 0.86	12.797 ± 0.064	4.52 ± 0.26	29.9 ± 6.8
^{185}Hg	2	40	3.13 ± 0.86	7.468 ± 0.066	4.41 ± 0.30	22.3 ± 6.2
^{185}Hg	5	0	3.13 ± 0.86	9.192 ± 0.048	4.96 ± 0.16	24.8 ± 6.4
^{206}Rn	0	0	3.36 ± 0.82	23.76 ± 0.14[a]	8.08 ± 0.46	46.7 ± 7.6[b]
^{206}Rn	2	0	3.36 ± 0.82	15.49 ± 0.11	7.41 ± 0.46	35.5 ± 7.0
^{206}Rn	2	20	3.36 ± 0.82	11.014 ± 0.050	4.95 ± 0.20	29.2 ± 6.6
^{206}Rn	2	40	3.36 ± 0.82	5.631 ± 0.082	3.81 ± 0.40	21.0 ± 6.0
^{206}Rn	5	0	3.36 ± 0.82	6.46 ± 0.11	8.8 ± 1.4	22.3 ± 6.2
^{254}No	0	0	2.12 ± 0.70	17.60 ± 0.18[a]	3.6 ± 1.4	29.0 ± 4.8[b]
^{254}No	2	0	2.12 ± 0.70	12.166 ± 0.084	1.32 ± 0.32	22.2 ± 4.4
^{254}No	2	20	2.12 ± 0.70	7.32 ± 0.15	2.29 ± 0.74	15.7 ± 3.8
^{254}No	3	0	2.12 ± 0.70	9.460 ± 0.072	2.7 ± 1.0	18.6 ± 4.0

[a] E_{M0} values for formula (3).
[b] E_0 values for formula (3).

the separator were comparable to those in the discovery experiments of element 114 [19]. The setup for the investigation of element 114 was designed as schematically depicted in Fig. 1. An RPC-chamber of 15 mm depth and otherwise same dimensions as given above was attached to the DGFRS separator. The gas-filled separator magnets and the RPC-chamber were separated by a Mylar foil of 3.0 μm thickness. The IVO loop setup was connected to this chamber using a 4 m perfluoroalkoxy-Teflon (PFA) capillary of 1.56 mm inner diameter. A drying unit kept the water content in the carrier gas below 0.01 ppm (dew point −101 °C), which represents the detection limit of the dew point sensors (Xentaur HTF) installed in the gas-loop system. The thermalized products were transported with an Ar carrier gas flow of 2.1 l/min at a pressure of 133 kPa to the Cryo-Online Detector (COLD) [13,20]. Only chemical species which are volatile at room temperature can pass the transport capillary. Thus an additional chemical separation of products was achieved. A temperature gradient between 10 °C and −170 °C was established along the COLD array. The detector sandwiches used consisted of two structurally identical PIPS diodes (active surface 9.7 mm × 9.7 mm). The PIPS diodes, which are in tight contact with the copper bar where the temperature gradient was established, are covered by a thin gold-layer (about 50 nm). The transported reaction products were deposited upon their interaction with the gold covered surfaces of these PIPS diodes in the COLD. The decay of deposited reaction products was registered by an event-by-event spectroscopy system using the MIDAS software package [21,22]. An ^{227}Ac (actinium) source emanating ^{219}Rn was used for the on-line calibration of the detectors and for a direct comparison of a noble gas deposition in the COLD with the chemical behavior of the superheavy elements. The cleanliness of the detector surfaces was periodically checked using ^{185}Hg. For this purpose, a $^{nat}Nd_2O_3$ target was used and the magnet settings were adjusted to transmit the ^{185}Hg to the focal plane of the separator. The broadening of the deposition pattern of the Hg along COLD was indicative of the beginning coverage of the gold surfaces by organic contaminants whose origin is as yet unknown. A cleaning procedure, subsequently applied with methanol, acetone, and diethyl ether reestablished the retention properties of the gold surfaces.

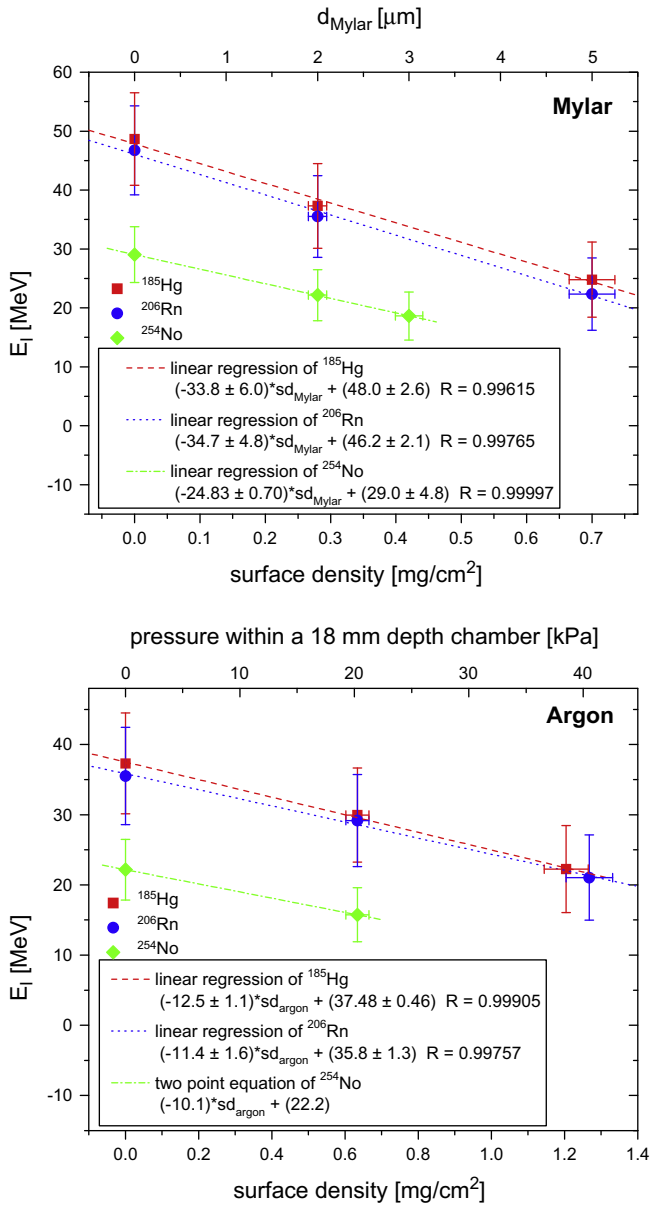

Fig. 3. Experimentally measured implantation energies of ^{185}Hg, ^{206}Rn, and ^{254}No corrected by PHD and the results of the least square fits. Upper graph: plot of E_I measured at 133 Pa H_2 pressure versus the Mylar window surface density (sd_{Argon}, lower axis) and foil thickness (upper axis) Lower graph: plot of E_I measured with a 2.0 μm Mylar foil prior to the gas volume versus the Ar surface density (lower axis) or Ar pressure in the RPC-chamber with a depth of 18 mm (upper axis). The lines represent the linear regressions with the appropriate equations to calculate the remaining energies of the evaporation residues in Mylar or Ar, respectively.

3. Results and discussion

3.1. Stopping force measurement

A typical spectrum of the PIN-diode signals of the STF-measurements is depicted in Fig. 2. The implantation signals of the EVR's (see Fig. 2, right panel) are clearly distinguishable from α-peaks in most of the spectra (see Fig. 2, left panel). The peak shapes were fitted with a Gaussian to determine the mean implantation energies of the EVR's see Fig. 2 right side. All uncertainties of this procedure and further uncertainties from calculations are given on a 2σ c.i. The energy spread of the EVR's leading to a full width at half maximum (FWHM) of about 8.1 MeV results from several factors: (1) the uncertainty of the beam energy and therefore of the primary recoil energy of the EVR's; (2) the straggling of the EVR's in the target material; (3) the individual trajectories of the EVR's through the DGFRS; (4) the angles at which the EVR's pass through the passive layer of the detector.

The measured implantation energies must be corrected for the pulse-height-defect (PHD) of the PIN-diodes used. According to [23,24] the electric field (i.e. reverse voltage) dependent part of the PHD is less important for ions heavier than ^{127}I and will be neglected. Therefore, Eq. (1) was used to describe the PHD (see Eqs. (14) and (15) in Ref. [23]). The true kinetic energy E_I (incident energy) of the EVR is deduced with Eq. (2) from the measured implantation signal E_M (mean energy) obtained with the α-calibration. The only free parameter in this parameterization that describes the PHD is the prefactor (*PF*) and that depends on the atomic-number (*Z*) and mass-number (*A*) of the implanted ions as well as on the structural specification of the detector used. This prefactor was deduced using Eq. (3) independently for each isotope from the measured implantation signal E_{M0} at DGFRS pressure conditions; i.e. without any additional thermalization of the ions. In this case TRIM-2008 [18], the simulation mode of SRIM-2008, was used to estimate the energy loss of the EVR's in the target material and in the gas-filling of the DGFRS plus RPC-chamber without a Mylar window. It was further assumed that the fusion reaction took place in the middle of the target. These results were

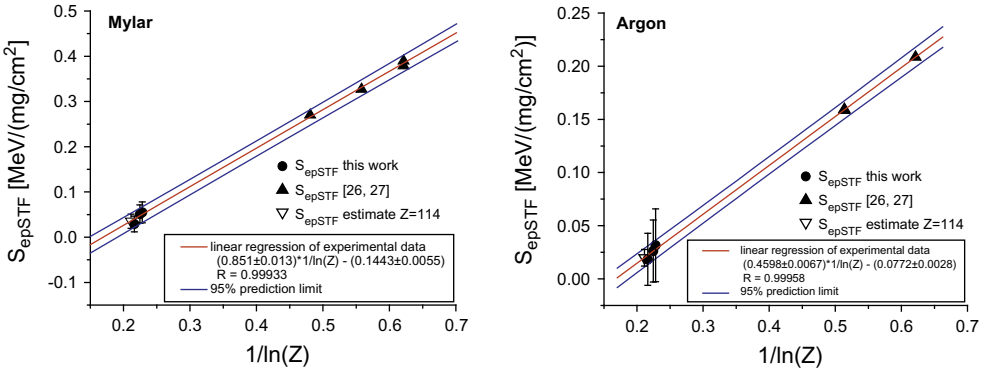

Fig. 4. The epSTF values from experimental data versus 1/ln(Z), as an empirical parameterization. The extrapolation of the epSTF in Mylar (left side, 86 keV per nucleon specific energy at entering the stopping medium) and Ar (right side, 36 keV per nucleon specific energy at entering the stopping medium) are shown. Points are from measurements of this work and triangles are data taken from Paul [26,27]. The full lines are the linear regression lines with the appropriate equation to calculate the epSTF belonging to ^{289}114. The outer lines represent the 95% prediction limits. The hollow symbol indicates the estimated value of Z = 114.

Table 4
Results of the extrapolation to the STF of element 114. In the third column are the experimental values of the STF's in Mylar (upper part) and gaseous Ar (lower part) as well as the ranges in the two media. The fourth and fifth column are SRIM-2008 results (see Section 3.3). In column four are the simulated values while in column five are the calculated values from "stopping/range tables" from SRIM-2008. The given uncertainties do not include experimental uncertainties of the stopping force data.

		^{289}114	SRIM ^{289}114	
		Experiment	Simulation	Table
In Mylar				
E_0	[MeV]	24.7 ± 4.0	24.7 ± 4.0	24.7 ± 4.0
STF	[MeV/(mg/cm^2)]	34.9 ± 15.4	29.7 ± 4.8	–
Range	[μm]	5.1 ± 2.4	6.0 ± 1.0	4.7 ± 0.8
		^{289}114	SRIM ^{289}114	
		Experiment	Simulation	Table
In Ar				
E_0	[MeV]	10.1 ± 7.6	10.1 ± 7.6	10.1 ± 7.6
STF	[MeV/(mg/cm^2)]	12.7 ± 4.6	19.5 ± 3.2	–
Range at 133 kPa	[mm]	3.5 ± 2.8	2.3 ± 0.4	2.5 ± 0.4

used to determine the initial incident energy E_0 of the EVR's, and thus to deduce the prefactor PF.

$$E_I - E_M = PF \cdot E_I^{1/2} \text{ where } PF \propto Z^{6/5} \cdot A^{7/10} \quad (1)$$

$$E_I = \left\{ \frac{PF}{2} \left(\sqrt{1 + \frac{4 \cdot E_M}{PF}} - 1 \right) \right\}^2 \quad (2)$$

$$PF = \frac{E_0 - E_{M0}}{\sqrt{E_0}} \quad (3)$$

To determine the uncertainties of the deduced mean incident energies an additional overall uncertainty of the particle spectroscopy electronics of 270 keV was assumed. In Table 2 E_M, E_I, FWHM, and the PF with their corresponding uncertainties are listed. All deduced uncertainties were obtained using the Gaussian error propagation principle including all discussed individual uncertainties as well as the uncertainties of further mathematical procedures (e.g. linear regression) used. In the latter case for the determination of the STF the individual uncertainties of the dependent variables were incorporated in the uncertainties of the deduced fitting parameters (see Table 3) as weighted uncertainties. For the two-point linear fit of the No data the uncertainties were estimated to be largest.

To determine the STF's and ranges of the ions in Mylar and Ar the determined EVR residual energy (i.e. the PHD corrected implantation energy, E_I) was plotted versus the foil thickness of Mylar or the surface density (i.e. mass divided by surface area) of Ar (Fig. 3). The STF's have been determined presuming their independence from energy within the used energy range. This assumption seems to be correct, see Fig. 3 from our experimental results at low energies between 50 keV per nucleon to 250 keV per nucleon. Obviously, the variability of the STF's at the applied experimental conditions is of minor importance compared to the uncertainties of the measurements due to the PHD-correction.

Thus, the slopes of the least square fits in Fig. 3 of the data yield the corresponding STF's of Mylar or Ar for ^{185}Hg, ^{206}Rn, and ^{254}No, respectively. From the extrapolation of the regression to zero residual energy the respective range (see [25]) of the ion was determined. This range represents the mean distance that the corresponding EVR's can travel with the incident energy E_0 in the stopping media Mylar and Mylar plus Ar, respectively. The stopping force values deduced from the experimental data for Mylar and Ar are compiled together with the corresponding ranges in Table 3.

3.2. Extrapolation to element 114

The measured STF values for Hg, Rn, and No were combined with other data from the literature [26,27] to permit extrapolation to element 114. Only the literature data of nitrogen, oxygen, carbon and boron are in the same velocity range as the measured data in this work. No uncertainties have been considered for these additional data points, because they are mostly missing in [26,27].

The extrapolations were made for ^{289}114 using the proportionality of the STF of the heavy ion to the square of effective charge and the *equivalent proton-STF* (in this case equivalent means that it has the same energy per nucleon or equivalent the specific energy), according to [28] it holds

$$-\left.\frac{dE}{dx}\right|_Z = q_{\text{eff}}^2(E_{\text{real}}, Z, A) \cdot \left[-\left.\frac{dE}{dx}\right|_{\text{eq. } Z=1} \right] = q_{\text{eff}}^2(E_{\text{real}}, Z, A) \cdot \text{epSTF} \quad (4)$$

The term dE/dx denotes the STF of any ion (Z) or the equivalent proton (eq. Z = 1) STF (epSTF) which is defined by Ziegler et al. [28]. The q_{eff} is the effective charge of the incident ion introduced by Northcliffe [29,30]. The velocity dependent factor of the effective charge λ that was used was defined by Sigmund [31]:

$$q_{\text{eff}} = \lambda Z e \quad (5)$$

$$\lambda = \sqrt{1 - e^{-v_1/v_{TF}}} \quad v_{TF} = Z^{2/3} v_0 = Z^{2/3} \cdot \alpha_{fs} \cdot c \quad (6)$$

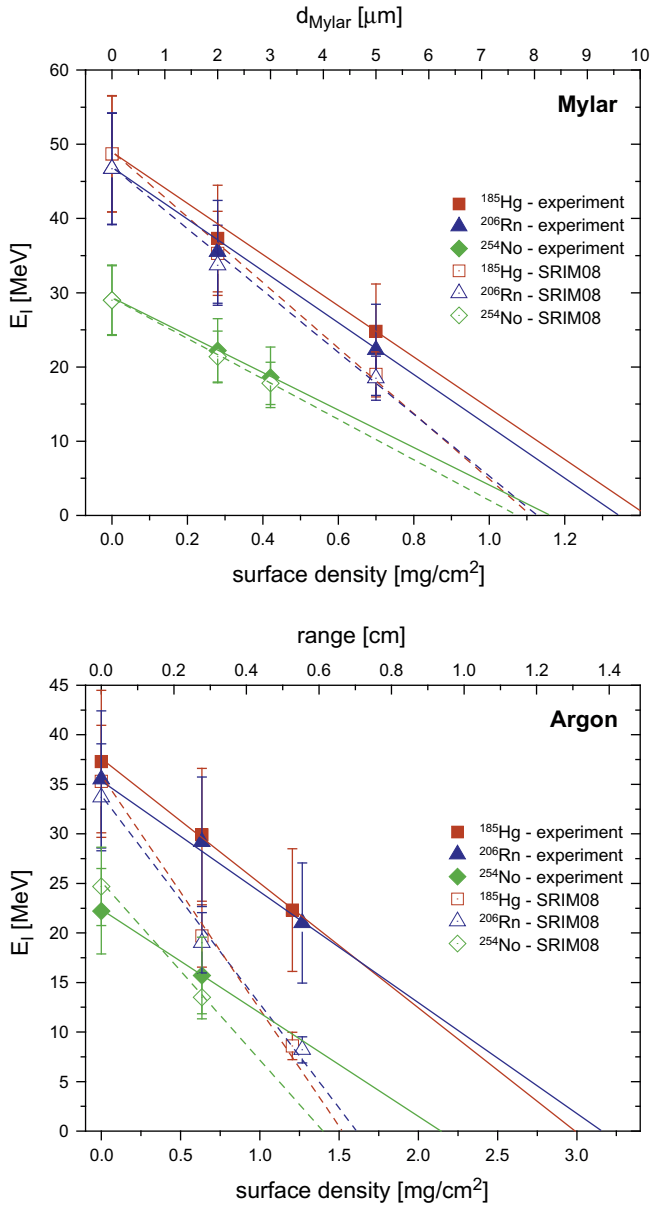

Fig. 5. Comparison of experimental data with TRIM simulations. Upper graph: plot of experimental (full symbols with full lines) and simulated TRIM-2008 (hollow symbols with dashed lines) data for ^{185}Hg, ^{206}Rn, and ^{254}No in Mylar. Top axis represents the thickness of the Mylar foil. The lower axis shows the corresponding surface densities. Lower graph: plot of experimental and simulated TRIM-2008 data for ^{185}Hg, ^{206}Rn, and ^{254}No in Ar. Top axis represents the mean range at 133 kPa pressure with the energy E_0. The lower axis shows the surface densities corresponding to this range. The lines in both graphs are drawn to guide the eye.

where v_{TF} is the Thomas–Fermi velocity, v_0 is the Bohr velocity, and α_{fs} the Sommerfeld fine structure constant.

E_0 of ^{289}114 was estimated by TRIM-2008. The incident energy of ^{289}114 isotopes for the Ar extrapolation was calculated by subtracting the energy loss in a 3.0 µm Mylar foil from the primary energy of the EVR's. Foils of this thickness were later used in the experiments with element 114. It should be noted that such an extrapolation requires the EVR's to have about the same incident velocity or specific energy.

Fig. 4 shows the extrapolation of the STF for element 114 in Mylar (left) and gaseous Ar (right). The resulting values were plotted against 1/ln(Z) which is an empirically deduced dependence of the STF.

The left side of Fig. 4 shows the extrapolation using the STF's for various elements in Mylar at the assumed velocity of ^{289}114 (specific energy: 85.5 ± 13.8 keV/u before entering the foil) behind the DGFRS separator. All data are within the 95% prediction limits or better. Experimental values from this work, Hg, Rn, and No were used together with data for boron, carbon, and oxygen taken from Paul [26,27] for the STF extrapolation in Mylar. The extrapolation to ^{289}114 (specific energy: 34.9 ± 26.3 keV/u before entering the gas volume) in the stopping medium Ar is shown on the right side of Fig. 4. The low Z data points are boron and nitrogen taken again from [26,27]. A linear relation between the epSTF values of the investigated isotopes and *1/ln(Z)* is observed for both stopping media.

Using the linear regressions from Fig. 4 the STF of element 114 can be calculated using the epSTF and the effective charge. The results of the stopping force calculation are compiled in Table 4. The stopping data for element 114 in Ar are derived for a setup with a 3 µm Mylar exit window foil and a 133 kPa pressure. These parameters were selected later for the experiment with element 114. These results indicate that behind a 3.0 µm thick Mylar foil the used RPC-chamber of 15 mm depth and flushed by Ar at a pressure of 133 kPa is a suitable setup to thermalize the ^{289}114 completely in the carrier gas volume at the assumed recoil energy calculated with TRIM-2008.

3.3. Comparison with SRIM-2008

The experimentally deduced STF's and stopping ranges were compared with values obtained using SRIM-2008 [18]. In the SRIM-2008 simulation Hg, Rn, and No passing through a virtual experimental setup were processed like the real experimental data (see above). The STF's and the ranges were derived. Because SRIM-2008 is not able to calculate ions with a higher atomic-number than uranium, a relation given by Ziegler et al. [28] (based on the eqSTF) was used to obtain the data for No and element 114.

$$S_{No} = S_U \frac{q^2_{eff,No}}{q^2_{eff,U}} \quad (7)$$

This relation requires that uranium and the wanted element have the same specific energy. It should be noted that according to [32], SRIM-2008 values have in general a 1σ uncertainty of around 8% in this energy region.

The results of this comparison between experimental data and SRIM simulation/calculation are shown in Figs. 5 and 6. SRIM ranges and STF's data of eka-lead are compiled in Table 4.

The experimentally deduced STF values and the data calculated with SRIM-2008 differ for Ar gas as stopping medium much more than for Mylar as stopping medium. Similar disagreements between experimental data and SRIM calculations of ranges of low-energy heavy ions in gases are discussed in [32]. This might be due to scarce experimental data for heavy ion stopping in gas, especially at such low energies. However, such data are needed to deduce the complete set of empirical parameters in SRIM and thus they are essential to obtain reliable estimates.

3.4. Experiment with element 114

Fig. 7 depicts accumulated and normalized α-spectra within the first 24 detector sandwiches of COLD array with and without using the DGFRS. A comparison with previously measured spectra without physical preseparation in the same reaction and at the same experimental conditions clearly indicates the significant suppression of unwanted events by several orders of magnitude. Especially important is the background reduction in the energy range above

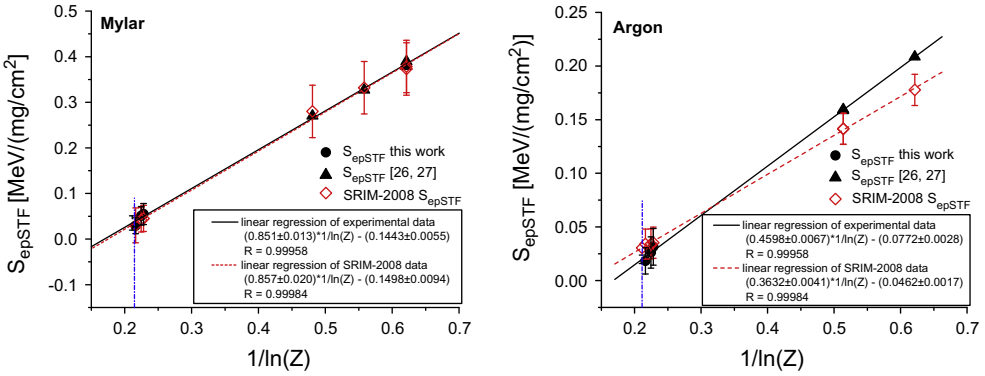

Fig. 6. Same data as in Fig. 4 (full lines) together with calculated values TRIM-2008 (dashed lines). The lines are the linear regression lines with the appropriate equations to calculate the epSTF belonging to ^{289}114. The position of element 114 is marked with a dashed-dotted line.

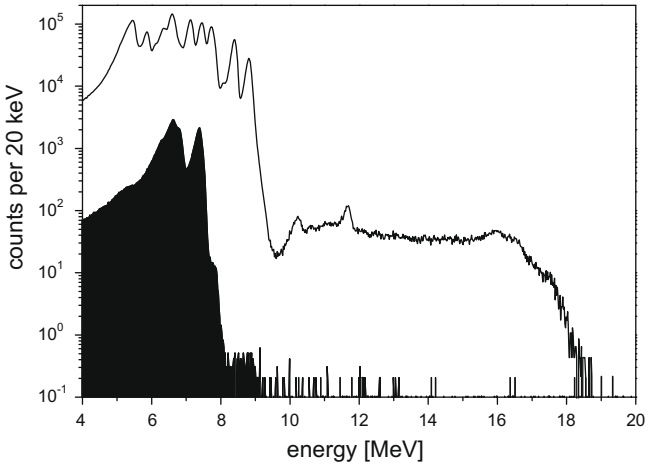

Fig. 7. Comparison of the α-sum (sum spectra from detector 1 to 27 of the COLD array [13,20]) normalized to the applied beam dose from experiments performed in 2007 [13,33] without preseparation (white spectrum) and with preseparation (black spectrum) [this work]. Both experiments used the nuclear reaction ^{48}Ca with ^{244}Pu and were performed at the same gas flow conditions. The data are normalized to the target thickness of 0.44 mg/cm^2 ^{244}Pu and 10^{18} ^{48}Ca particles.

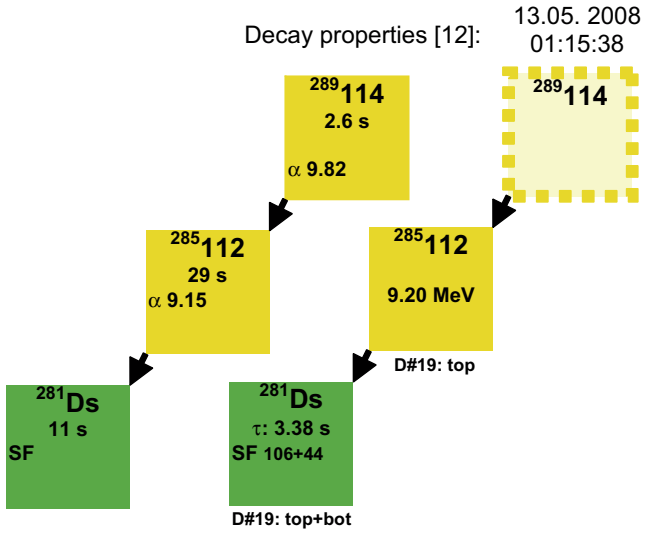

Fig. 8. Published decay properties of ^{289}114 from [1] (left side). The right chain depicts the decay chain observed during the experiment.

9 MeV, where most of the α decays of super heavy elements are expected.

This gain in background suppression is however accompanied by a loss in overall sensitivity, as already discussed.

In the course of the experiment, 17 single high energy events over 50 MeV were detected, mostly originating from fast particles and/or electronic noise. Because the probability to detect only one fragment of a spontaneous fission (SF) is 37% in the COLD array [33], it is very unlikely (total probability rate about 3.1×10^{-6}) that all of them originate from real SF-decaying isotopes.

During the experiment one decay chain was observed that can be attributed unambiguously to the decay of ^{285}112 and its daughter ^{281}Ds (Fig. 8, right side), which are the descendants of ^{289}114. From the sum of α-spectra (Fig 7, black) and the amount of high energy events above 50 MeV in the detectors throughout the experiment (see below) the number of expected random correlations during the entire experiment was estimated to be 1.8×10^{-3} [34]. The decay of ^{285}112 takes place in the COLD array on detector #19 held at a temperature of −93 °C. The observation can be explained by the decay of an adsorbed atom of ^{285}112, which was produced in the α-decay of the reaction product ^{289}114 during transport from the RPC-chamber to the COLD array. Based on the known adsorption properties of element 112 on gold [13,14] and using the Monte-Carlo model of gas chromatography [35] one can estimate that about 21% of ^{285}112 are able to reach or pass detector #19 under the used experimental conditions. On the other hand the observed decay chain might be just incomplete because the α particle from the ^{289}114 decay was missed. The probability to miss the α particle in this decay chain was expected to be 28% in the COLD array [33]. Then, the observation would represent the chemical deposition of element 114 at −93 °C temperature on a gold surface indicating a high volatility and chemical inertness of element 114 as it was observed before [33].

In addition two clear SF events with coincident fragment detection have been observed in detectors 4 (−8 °C, fragment energies 131 MeV and 50 MeV) and 6 (−16 °C, 88 MeV and 101 MeV), respectively (see Fig. 9). Under the justified assumption that the physical preseparation and the additional chemical separation completely suppressed actinides, we tentatively assign these events to transported $^{288-289}$114 or their progenies, as the only sources of SF events. However, no unambiguous identification of the nuclide is possible through the mere detection of an unspecific SF-decay.

The detection of super heavy elements in the COLD confirmed the STF estimations elaborated in this work.

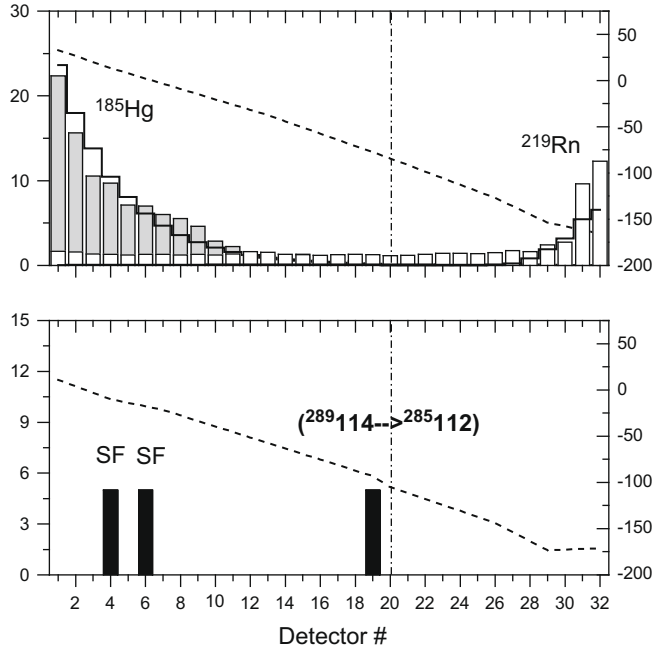

Fig. 9. The thermochromatographic deposition patterns of ^{185}Hg, ^{219}Rn, and the observed events attributed to transactinides in the COLD array at the established experimental conditions. Measured ^{185}Hg (grey bars), and ^{219}Rn (white bars) are shown together with the relative yield distribution for ^{185}Hg and ^{219}Rn as a function of the detector number as expected by a microscopic model of the adsorption chromatographic process based on a Monte-Carlo approach [35] (solid black line, left handed axis) using the adsorption enthalpies of Hg on gold (−98 kJ/mol) from [36] and Rn on ice (−19 kJ/mol) from [37]. The vertical dashed-dotted lines indicate the onset of ice formation the gold surfaces deduced from a permanent dew point measurement in the carrier gas using Xentaur HTF sensors. A temperature gradient from +11 to −170 °C was established along COLD array (right hand axis).

Acknowledgements

We thank the staff of the U-400 cyclotron for providing intense beams of ^{48}Ca. The ^{244}Pu target material was provided by the U.S. DOE through ORNL, Oak Ridge, USA. The LLNL work was performed under the auspices of the US Department of Energy by Lawrence Livermore National Laboratory (contract: DE-AC52-07NA27344). This work was supported in part by the Russian Foundation for Basic Research (Grants: 07-03-00430-a, 07-02-00029-a) and by the Swiss National Science Foundation (Grant: 200020-117671/1).

References

[1] Yu.Ts. Oganessian, J. Phys. G 34 (2007) R165.
[2] M. Schädel, Angew. Chem. Int. Ed. 44 (2005) 2.
[3] J.P. Omtvedt et al., Eur. Phys. J. D 45 (2007) 91.
[4] R. Sudowe et al., Radiochim. Acta 94 (2006) 123.
[5] G. Münzenberg et al., Nucl. Instr. and Meth. 161 (1979) 65.
[6] A.V. Yeremin et al., Nucl. Instr. Meth. A 274 (1989) 528.
[7] V. Ninov, K.E. Gregorich, in: B.M. Sherrill, D.J. Morrissey, C.N. Davids (Eds.), ENAM98, AIP, Woodbury, 1999, p. 704.
[8] Yu.Ts. Oganessian et al., in: Proceedings of Fourth International Conference on Dynamical Aspects of Nuclear Fission, 19–23 October 1998, Častá-Papiernička, Slovak Republic, World Scientific, Singapore, 2000, p. 334.
[9] K. Morita et al., Eur. Phys. J. A 21 (2004) 257.
[10] A. Semchenkov et al., Nucl. Instr. and Meth. B 266 (2008) 4153.
[11] M. Leino, Nucl. Instr. and Meth. B 204 (2003) 129.
[12] Ch.E. Düllmann et al., Nucl. Instr. and Meth. A 479 (2002) 631.
[13] R. Eichler et al., Angew. Chem. Int. Ed. 47 (2008) 3262.
[14] R. Eichler et al., Nature 447 (2007) 72.
[15] Yu.Ts. Oganessian et al., Phys. Rev. C 72 (2005) 034611-1.
[16] R. Dressler, Paul Scherrer Institut (PSI) Scientific Report 1998, vol. I, 1999.
[17] K. Subotic et al., Nucl. Instr. and Meth. A 481 (2002) 71.
[18] J.F. Ziegler, J.P. Biersack, U. Littmark, SRIM-2008, http://www.srim.org, 2008.
[19] Yu.Ts. Oganessian et al., Phys. Rev. C 62 (2000) 041604.
[20] R. Eichler et al., Radiochim. Acta 94 (2006) 181.
[21] S. Ritt, MIDAS, http://midas.psi.ch, 2001.
[22] R. Dressler, Paul Scherrer Institut (PSI) Scientific Report 2002 (2003) 131.
[23] M. Ogihara et al., Nucl. Instr. and Meth. A 251 (1986) 313.
[24] V. Zajic, P. Thieberger, IEEE Trans. Nucl. Sci. 46 (1999) 59.
[25] P. Sigmund, Stopping of Heavy Ions – A Theoretical Approach, Springer Tracts in Modern physics, vol. 204, Germany, 2004.
[26] H. Paul, A. Schinner, Nucl. Instr. and Meth. B 179 (2001) 299.
[27] H. Paul, A. Schinner, Nucl. Instr. and Meth. B 195 (2002) 166.
[28] J.F. Ziegler, J.P. Biersack, U. Littmark, The Stopping and Range of Ions in Solids, Pergamon Press, Kronberg-Taunus, Federal Republic of Germany, 1985.
[29] L.C. Northcliffe, Phys. Rev. 120 (1960) 1744.
[30] L.C. Northcliffe, Ann. Rev. Nucl. Sci. 13 (1963) 67.
[31] P. Sigmund, Phys. Rev. A 56 (1997) 3781.
[32] H. Paul, A. Schinner, Nucl. Instr. and Meth. B 209 (2003) 252.
[33] R. Eichler et al., Radiochim. Acta, submitted for publication.
[34] K.H. Schmidt et al., Z. Phys. A 316 (1984) 19.
[35] I. Zvara, Radiochim. Acta 38 (1985) 95.
[36] S. Soverna et al., Radiochim. Acta 93 (2005) 1.
[37] B. Eichler, P. Zimmermann, H.W. Gäggeler, J. Phys. Chem. A 104 (2000) 3126.